ACS APPLIED BIO MATERIALS

www.acsabm.org Letter

Design Principles of Lipid-like Ionic Liquids for Gene Delivery

David J. Siegel,[†] Grace I. Anderson,[†] Lauren M. Paul, Philipp J. Seibert, Patrick C. Hillesheim, Yinghong Sheng, Matthias Zeller, Andreas Taubert, Peter Werner, Christian Balischewski, Scott F. Michael,* and Arsalan Mirjafari*

Cite This: *ACS Appl. Bio Mater.* 2021, 4, 4737–4743 Read Online

ACCESS | Metrics & More | Article Recommendations | Supporting Information

ABSTRACT: We developed lipid-like ionic liquids, containing 2-mercaptoimidazolium and 2-mercaptothiazolinium headgroups tethered to two long saturated alkyl chains, as carriers for in vitro delivery of plasmid HEK DNA into 293T cells. We employed a combination of modular design, synthesis, X-ray analysis, and computational modeling to rationalize the self-assembly and desired physicochemical and biological properties. The results suggest that thioamide-derived ionic liquids may serve as a modular platform for lipid-mediated gene delivery. This work represents a step toward understanding the structure−function relationships of these amphiphiles with long-range ordering and offering insight into design principles for synthetic vectors based on self-assembly behavior.

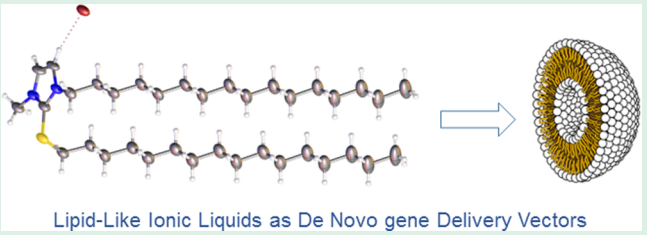

KEYWORDS: *DNA delivery, cationic lipids, nonviral vectors, ionic liquids, gene therapy, lipid-like materials, biomaterials*

First introduced in Friedmann and Roblin's 1972 seminal article,[1] gene therapy has since been a topic of scientific interest as a promising strategy to treat various monogenic disorders.[2−5] Although viral vectors are more common in gene delivery because of their relatively high delivery efficiency, their immunogenicity and generalized toxicity impose major obstacles to the clinical success of gene therapy.[6] In turn, these challenges have shifted attention to the incorporation of new design elements for more efficient and safe nonviral synthetic vectors to transfer nucleic acid-based therapeutics into target cells. Although this strategy has resulted in advances toward functional carriers, only 4.2% of clinical trials involving viral or nonviral carriers have reached a late clinical phase.[7]

Gene therapy represents an area where appropriate molecular design is critical to achieve a successful outcome. The paradigm of the development of synthetic gene delivery vectors with viral-like efficacy relies on the rational design of biomaterials through the incorporation of precise structural characteristics for effective and specific transfection—an imperative, albeit slow process.[6] Underlying this goal is the additional desire to develop efficient, modular, and scalable synthetic strategies that ideally fit into the conceptual framework of sustainability.

Cationic lipids (or cationic liposomes) were investigated as nonviral gene delivery agents because of their reduced immunogenicity, low cytotoxicity, ease of manufacturing, and large payload of DNA polynucleotides[8−12] (i.e., up to 20 000 bp of plasmid DNA were encapsulated and delivered without obstructing the transfection efficiency[13]). DOTMA and its congeners (Figure 1) are classic examples of cationic lipid carriers introduced by Felgner et al. in 1987, as "simple, highly reproducible, and more efficient than some other, commonly-used procedures".[14] Thereafter, a variety of cationic liposomes that resemble the overall structure of DOTMA were developed (Figure 1).[15] DOTMA-type compounds generally consist of three distinct structural subcomponents: (i) an ammonium headgroup that provides a locus of cationic charge, facilitating electrostatic binding to anionic DNA; (ii) a glyceryl moiety,

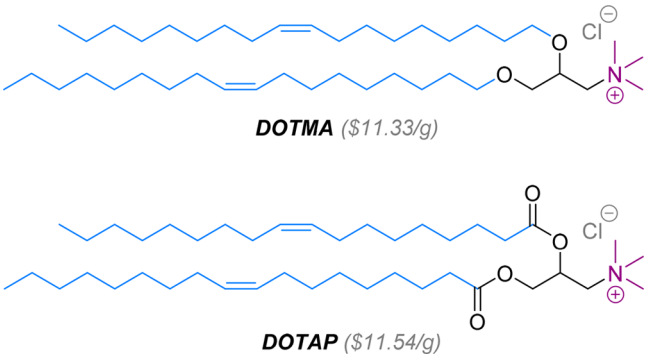

Figure 1. Structures of commercially available DOTMA and DOTAP. Structural moieties include a cationic headgroup (purple), ether/ester backbone (black), anion (gray), and paired lipidic tails (blue).

Received: February 27, 2021
Accepted: June 1, 2021
Published: June 2, 2021

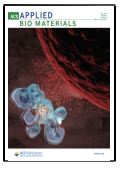

https://doi.org/10.1021/acsabm.1c00252
ACS Appl. Bio Mater. 2021, 4, 4737–4743

Scheme 1. Single-Step Synthesis of LILs, Containing Heterocyclic Headgroups (Purple), a Thioether Linker (Black), and Hydrophobic Tails (Blue)

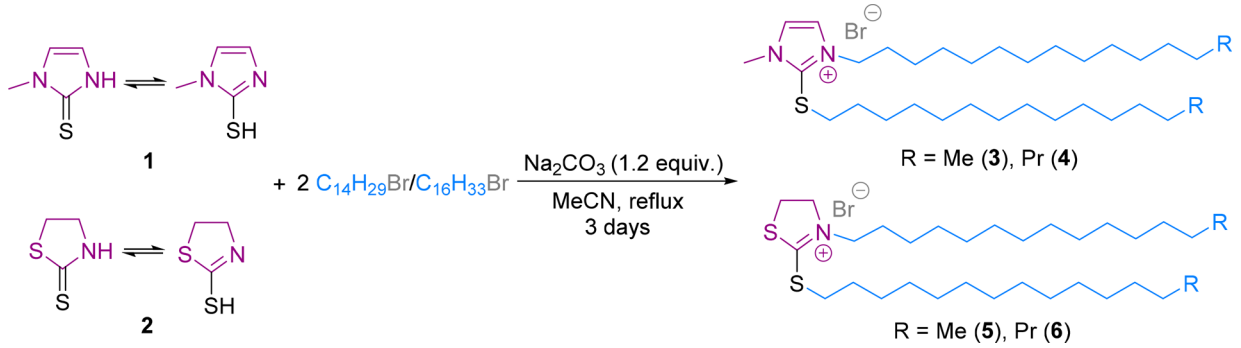

which provides a covalent bridge between the headgroup and the final substructure; and (iii) two aliphatic chains, each tethered to the glyceryl moiety via an ether or ester linker. Regardless of their nature (saturation vs unsaturation), the hydrophobic association of these tails facilitates the self-assembly of the liposome. Markedly, the transfection efficiency is correlated to those specific structural loci.[16]

In our prior work,[17] using thiol−yne chemistry, we developed ammonium- and imidazolium-based lipid-like ionic liquids (LILs) with C_{12} and C_{14} saturated tails and thioether linkers for DNA delivery.[17] The transfection efficiency of amphiphiles with the aromatic headgroup were superior to their nonaromatic analogs, forming well-packed lamellar structures that impart stability to lipoplexes. Furthermore, incorporating the lipophilic thioether backbone (in lieu of glycerol) extended the hydrophobic domain, effectively moving the polar/nonpolar interface to the level of the headgroup, ultimately enhancing self-assembly.

In our search for promising synthetic vectors to transfect DNA, we synthesized a series of LILs wherein hydrocarbon chains are directly bound to the cationic headgroup (Scheme 1, **3**−**6**) with 2-mercaptoimidazole **1** as the cationic moiety (commonly referred to as methimazole, a common antithyroid drug[18]) and 2-mercaptothiazoline **2**. The restrictive conformational freedom of the thioamide-derived headgroups[19] was expected to confer an elongated linear shape, allowing more compact packing alongside improved self-assembly into lamellar phases. Further, it is expected that the extended positive charge delocalization throughout the 2-mercaptoimidazolium cation[19] (**3** and **4**) leads to increased hydrophobicity of the nonpolar domain, enhancing the self-assembling ability of the amphiphiles, cf. ammonium headgroups. Our proof-of-concept study identified these materials for their efficient condensation and release of plasmid DNA in vitro into HEK 293T cells, an epithelial line derived from human kidney tissue. The experimental values of melting points (T_m) for the LIL products indicate that all fall below the customary benchmark of 100 °C,[20] which is commonly used to categorize a salt as an IL (vide infra).

In our de novo design, we incorporated three structural elements: (i) thioamide-derived charge-delocalized heterocycles as cationic headgroups; (ii) a thioether linker to bridge an aliphatic chain to the headgroups; and (iii) paired myristyl and palmityl chains as the hydrophobic anchor. This convergent synthetic strategy has at its core the facile generation of the polar headgroups and linkers through the dialkylation of heterocycles **1** and **2** with myristyl/palmityl bromides in a single, high-yield step (Scheme 1). Incorporation of a nonaromatic headgroup into our design strategy further serves to broaden structural diversity. Notably, the modular design provides a versatile platform to develop structurally diverse cationic lipids based on three considerations: (i) starting materials are inexpensive and commercially available; (ii) *N*,*S*-dialkylation can be achieved directly in a single step, producing LILs in excellent yields; and (iii) since no byproducts are generated, no chromatographic purification is required.

Generally, the capability of ILs to promote amphiphilic self-assembly into a range of mesophase structures has been recognized as a well-established phenomenon.[21] ILs with long side chains are inherently amphiphilic and can self-assemble into nanostructures, segregating into polar and nonpolar domains to form a nanostructured liquid.[22] In this work, the self-assembling properties of the LILs **3**−**6** were studied via a combination of single-crystal X-ray diffractometry (SC-XRD), differential scanning calorimetry (DSC), and computational approaches, establishing the thermotropic and lyotropic supramolecular assemblies of these amphiphiles. These studies provide a route to evaluating the strength of the supramolecular assemblies of the lipids in bulk forms, which is relevant for the ease of lipoplex preparation and stability.

To assess the long-range ordering of the structures, we acquired the solid-state structure of LIL **4** via SC-XRD. The molecules displayed self-organization through distinct noncovalent interactions (i.e., coulomb and van der Waals forces) and formed an interdigitated bilayer-structure via the clear segregation of polar and nonpolar domains (Figure 2). The alternating rod-shaped cations and anions arrange in a parallel alignment. We previously reported that the inclusion of sulfur

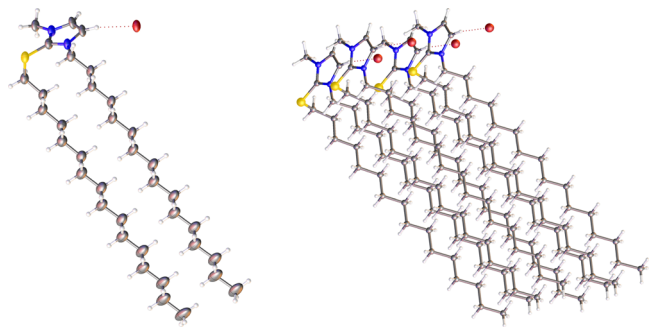

Figure 2. Single-crystal structure (left) and packing diagram (right) of the LIL **4**.

https://doi.org/10.1021/acsabm.1c00252
ACS Appl. Bio Mater. 2021, 4, 4737−4743

groups in the alkyl chains of LIL tends to form gauche conformations.[23] This is readily evident in the alkyl chain on the thioether group on the C2 position of the ring. The C2—S1—C7A—C8A torsion angle is 65.1(7)°. This gauche conformation facilitates intramolecular C···H|H···C interactions between the alkyl tails while controlling the intermolecular structuring. The molecules are oriented in a manner to allow interactions between adjacent alkyl chains, which extend in three dimensions, effectively creating lipophilic regions (Figure 2, left).

As a borderline kosmotropic anion, Br^- is associated loosely with the polar headgroup of the amphiphiles. As expected from aromatic-based ILs, the shortest interactions with the halide anion arise from aromatic hydrogens on the methimazolium ring with the shortest halide contact at C5—H (d = 2.6434(15) Å). The bromide also acts as a bridge between the C4—H and C6—H interacting with both hydrogens at distances of 3.0883(13) and 3.0141(13) Å, respectively.

To obtain a detailed picture of these interactions in **4**, we performed a Hirshfeld surface analysis using the *CrystalExplorer* software[24] (Figure 3). The analysis indicated that the

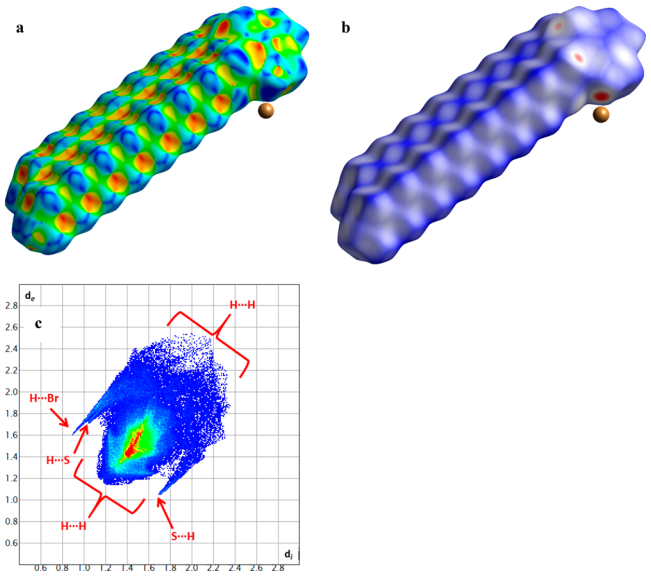

Figure 3. Hirshfeld surface mapped with (a) the shape index, (b) d_{norm}, and (c) fingerprint plot of the LIL **4**.

relative percentages of interactions for H···All, H···H, H···Br, H···S|S···H and H···C|C···H are 95.9, 88.9, 4.4, 3.0, and 1.9%, respectively. As expected, H···H interactions between two tails comprise ca. 89% of all close contacts between molecules. These interactions are seen in the fingerprint plot (Figure 3) as the main "bulk" of the plot ranging from $d_i \approx d_e \approx 1.2$ to the disperse points at $d_i \approx d_e \approx 2.4$. The bright red portion of the image visualizes the largest number of interactions at $d_i \approx d_e \approx 1.5$. The dominant H···H alkyl interactions are also evident in the shape index surface (Figure 3). The characteristic alternating blue/red pattern along the top and sides of the surface show how the C−H groups pack together to maximize the alkyl interactions. There are three total H-interaction "spikes" seen in the fingerprint plot (Figure 3). The topmost spike, starting at d_i = 0.9, d_e = 1.6, is from the H···Br interactions with the aromatic and alkyl hydrogens (vide supra). The other two spikes arise from the reciprocal set of H···S|S···H sets of interactions (d_i | d_e = 1.7 | 1.1). Two shorter S···H interactions (2.83−2.85 Å) are seen arising between the sulfur and C−H moieties on symmetry adjacent alkyl chains. These interactions are seen in both the d_{norm} surface and shape index as the red points of contact (Figure 3). These S···H interactions are not uncommon and are of importance in the formation of structures in biological systems.[25] It follows that these S···H interactions also play a role in the formation of long-range ordering of the complexes by interacting with hydrogens on both alkyl chains.

Density functional theory (DFT) modeling provides a clear picture of self-assembly of the LILs. The self-assembly of LILs **4** and **6** is presented in Figure 4 and Figure S1. The analysis of this assembling behavior is important because it allows one to evaluate the strength of the supramolecular assemblies of lipids in the dehydrated form, which is relevant for ease of liposomal formulation and lipoplex stability. LILs **4** and **6** form an elongated linear shape, allowing packing into the lamellar phase and formation of cationic bilayers (Figure 4, top). This is consistent with the electrostatic surface of the cations (Figure 4, bottom). Dictated by the adopted cylindrical-shape conformation of LILs **4** and **6**, the boundary between the hydrophilic/hydrophobic domains is positioned at the level of the headgroups.

The DSC analysis was performed to assess the self-assembling properties of the LILs in bulk and hydrated forms. As noted, various self-assembling dynamics were observed for aromatic LILs **3** and **4**, exhibiting the multi-featured traces characteristic of lipoids (Figure 5), which is

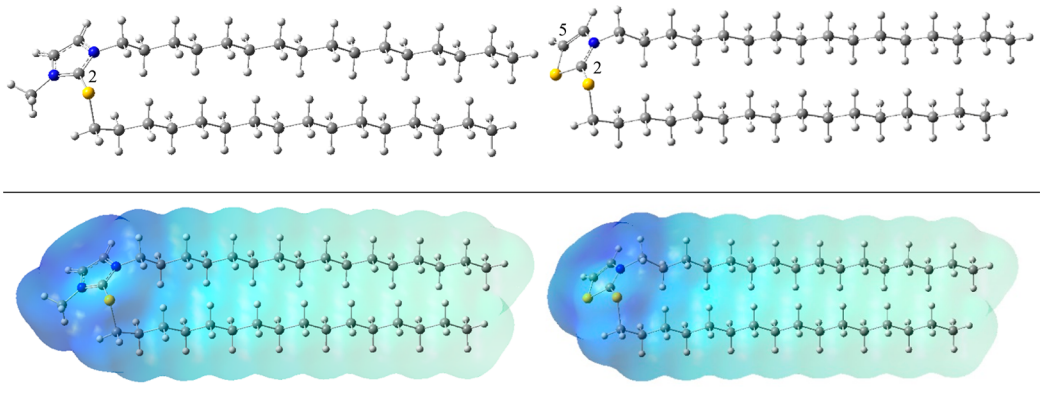

Figure 4. DFT optimized structures of cations from LILs **4** and **6** (above) along with their electrostatic potential maps (below).

https://doi.org/10.1021/acsabm.1c00252
ACS Appl. Bio Mater. 2021, 4, 4737−4743

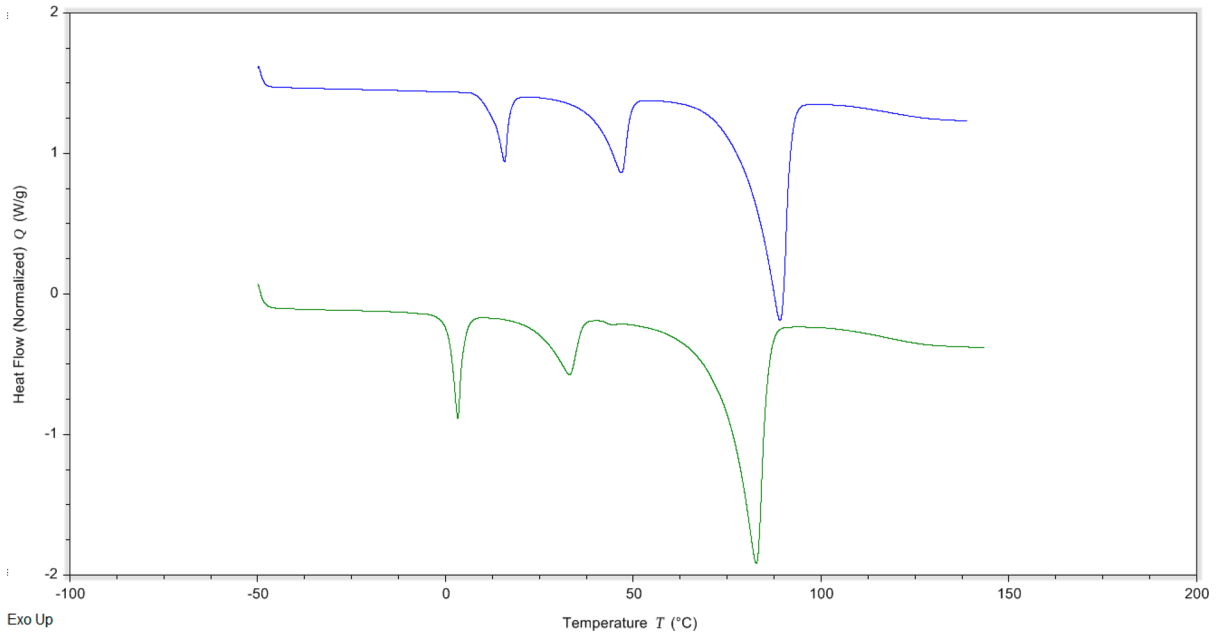

Figure 5. DSC thermograms for compounds **3** (green) and **4** (blue) of second heating/cooling cycle. The thermograms were offset along the heat flow axis for clarity but not rescaled (starting point is zero for both scans).

often the case for ILs[26] and lipids.[27] In addition, the T_m values (or isoteropization temperature) of the products were determined by DSC with a heating/cooling rate of 5 °C/min, within the temperature range of −50 to 150 °C. The isotropization temperatures of **3**−**6** are 73.6, 78.9, 48.9, and 69.7 °C, respectively, which provide a solid basis for their definition as classical ILs (see the Supporting Information for DSC thermograms of the products). A possible explanation for these low melting temperatures is that the kosmotropic bromide anion tends to push its minimum energy position to a larger separation from the polar/nonpolar interface, weakening the electrostatic interactions with the positively charged headgroups and decreasing melting points. Interestingly, the nonaromatic LILs show lower T_m values (ΔT_m = 9.2 −24.7 °C) compared to their aromatic congeners. This is perhaps due to the presence of the sulfur atom within the ring, diminishing the tight molecular packing and making the bilayer more fluid.[28]

These LILs were hydrated using the standard freeze−thaw procedure[15] to generate the multilamellar vesicles (MLV), then sonicated to form the single lamellar vesicles (SLV). As expected, the transition temperatures decreased in the hydrated form, as compared with the thermotropic case, due to the reduced interbilayer cohesion of the cationic amphiphiles. Similar to the thermotropic case, the elongation of the tails drastically affected the transition temperatures of the SLVs.

Using thermogravimetric analysis (TGA), the thermal decomposition temperatures ($T_{decomp.}$) of the products were measured by heating the sample from room temperature to 350 °C. The TGA data showed an initial decomposition step (onset decomposition temperature) between 144.6 and 201.4 °C (see the Supporting Information), indicating significant mass loss (ca. 45−48%). Predictably, these ILs exhibit low thermal stability due to the strong nucleophilicity of the halide anion.[29]

The ability of LILs **3**−**6** to complex pDNA was qualitatively evaluated by an agarose gel electrophoresis shift assay. Because of the poor solubility of the LILs in water at pH 7.4 in the desired concentrations, DNA−LILs complexes were prepared using DMSO and the resulting complexes remained soluble upon dilution in the running buffer for electrophoresis. Data were obtained at physiological pH and the results are shown in Figure S4 (see the Supporting Information) for a range of LILs:DNA weight ratios. Partial inhibition of DNA migration is seen at all LIL−DNA ratios. This trend indicates that increasing amounts of LILs are essential to bind to DNA more effectively. Surprisingly, among the LILs, only **5** can efficiently compact pDNA in 1:4 ratios without having the positive charge diluted by colipids. This is perhaps due to the fact that the gel electrophoresis assay does not precisely reproduce the LIL/DNA binding environment of the actual transfection experiment. Moreover, the lower solubility of aromatic LILs **3** and **4** may be responsible for their poor uptake level, limiting their interaction with DNA.

The zeta potential values indicate generally great stability in the liposomal dispersion of the target ILs in water. Interestingly, LILs **3** and **4** displayed positive zeta potentials of +38.38 and +62.49 mV, respectively, whereas **5** and **6** displayed negative zeta potential measurements of −21.75 and −32.13 mV, respectively (Figure S5). This positive surface potential for LIL **3** and **4** correlates with the biological data showing these ILs as having higher transfection efficacy, likely due to charge neutralization. Moreover, LIL **4** was the most effective transfection vector, simultaneously demonstrating a higher zeta potential than the others, indicating stronger nanoparticle aggregation and stability as part of its transfection capabilities. This unique feature was displayed by many heterocyclic amphiphiles with delocalized cationic charge,[15] allowing simplification of the formulation process and yielding more homogeneous lipoplexes.

The quantitative assessment of the in vitro transfection efficiency of the resultant LILs was achieved using the previously described optimized experimental conditions.[17] The LILs were tested for their ability to deliver DNA plasmid, expressing green fluorescent protein ($pCMV_{ie}eGFP$) in 293T

https://doi.org/10.1021/acsabm.1c00252
ACS Appl. Bio Mater. 2021, 4, 4737−4743

cells, with transfection values at the optimized conditions shown in Figure 6. These results were compared to poly-L-lysine (PLL) alone and Mirus Bio *Trans*-IT 293, a commercially available reagent. PLL has been widely studied as a DNA condensing agent and is the standard to which new vectors are often compared.[30] PLL was used it as a model cocomplexing agent in this study and it was selected because it is a relatively poor transfection agent on its own. Reasonable levels of transfection were observed for all the LILs relative to a naked DNA control experiment, but the level of gene expression was lower than for the Mirus Bio *Trans*-IT 293 (ca. 19−31%). The transfection efficiencies of LILs **3** and **4** were found to be superior to its congener with nonaromatic headgroups, likely due to the presence of stronger electrostatic interactions of the aromatic headgroups with DNA. We found that the lipofection capability of these cationic amphiphiles increase with chain length (**3** vs **4**). We also made a methimazolium-based salt with two stearyl tails (not shown in Scheme 1), which was difficult to formulate because of its poor solubility even after repeated freeze−thaw and sonication cycles. We were not able to generate stock solutions of this salt with adequate concentrations. As shown in Figure 6, the LIL **4** is our lead candidate, demonstrating the highest efficiency to cytotoxicity ratio. The assay system described above can be readily tuned. Additional investigations will be required to more fully evaluate the potential of this screening library. Experiments to this end are currently underway.

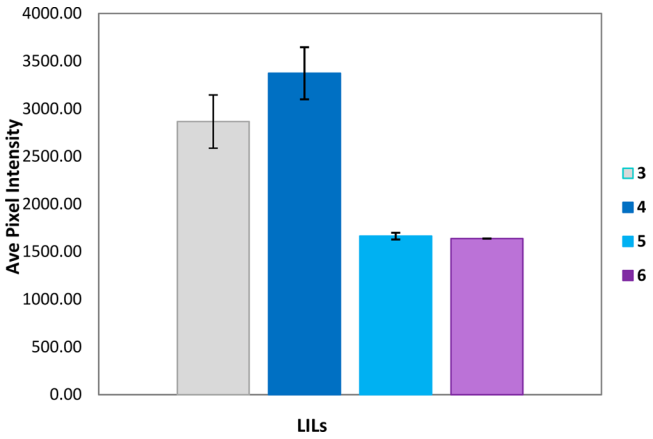

Figure 6. Transfection efficiency of the LILs, employing pDNA ($pCMV_{ie}eGFP$) into HEK 293T cells. The concentrations of LIL **3**, **4**, **5**, and **6** are 189 μM, 167 μM, 3.3 mM, and 3 mM, respectively. The standard samples without LILs (naked pDNA and DNA−PLL) showed no efficacy.

Further assessment of the transfection capabilities of the LILs was achieved by confocal microscopy, observing intracellular distribution of plasmid-expressed GFP in HEK 293T cells. As shown in Figure 7, the fluorescing green cells appear throughout the field of view for transfections using LIL products, suggesting efficient cellular uptake of the LILs.

To determine the cytotoxicity profile of the resulting amphiphiles and LIL−PLL−pDNA complexes, we performed the standard MTT and the CellTiter-Glo cell viability assays, respectively (see Figures S6 and S7). First, the standard MTT test was used to determine metabolic activity of LLC-MK2 cells in the presence of various LIL concentrations (Figure S6). LILs **3**−**6** exhibited promising biocompatibility even in high

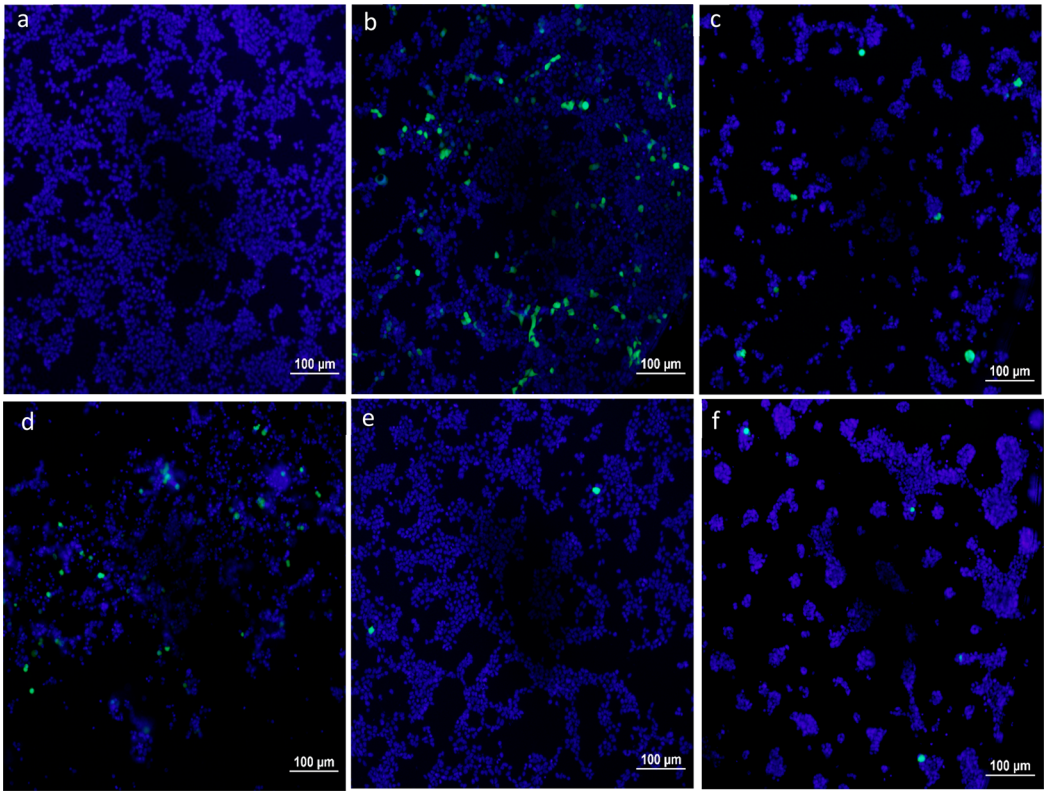

Figure 7. Confocal microscopy images of human 293T cells transfected with 1 μg of $pCMV_{ie}eGFP$ in conjunction with PLL to express green fluorescent protein using different reagents: (a) PLL alone, (b) Mirus Bio *Trans*-IT-293 alone, (c) LIL **3** (189 μM), (d) LIL **4** (167 μM), (e) LIL **5** (3.3 mM), and (f) LIL **6** (3 mM).

https://doi.org/10.1021/acsabm.1c00252
ACS Appl. Bio Mater. 2021, 4, 4737−4743

concentrations, i.e., the TC_{50} values for LILs **3**–**6** are ca. 0.1, 0.3, 3.6, and 7.2 mM, respectively. Additionally, the CellTiter-Glo was employed to measure the cytotoxicity LIL–PLL–pDNA complexes. Although the differences in cytotoxicity may make a direct structure–function-based comparison between the LILs, their promising toxicity profiles confirm that they are viable candidates for further study as DNA condensing agents. As shown, the LILs **3** and **4** show great biocompatibility even at high concentrations. Cell viability reduced linearly as the ratio was increased.

In summary, the present work presents a one-step synthesis of four new lipid-like ILs as efficient gene transfection vectors with low toxicity. The incorporation of long alkyl groups into the 2-mercapto-based heterocycles using this divergent approach constitutes a facile and inexpensive route to produce various cationic lipids. The extended hydrophobic domain and conformational rigidity of cationic headgroups play a determinative role in self-assembly of the LILs. Because of their optimized hydrophilic/hydrophobic interface, these LILs can readily self-assemble in bulk and hydrated form, forming cationic bilayers to efficiently deliver DNA into the targeted cell, proven by structure–property–function relationship studies.

Finally, although our findings focused on four example LILs, structurally similar cationic lipids can be easily tuned for safer and more efficient vectors. This work lays the foundation to design "better" biomaterials for the gene delivery application through elucidation of fundamental design considerations. Further experiments are underway to fine-tune these backbones via variation of the aromatic headgroups and side chains in our laboratories.

■ ASSOCIATED CONTENT

Supporting Information

The Supporting Information is available free of charge at https://pubs.acs.org/doi/10.1021/acsabm.1c00252.

Experimental procedures and characterization data; synthesis; crystallographic data; experimental setup for transfections and cytotoxicity; gel electrophoresis; zeta potentials data; spectra; and DSC and TGA thermograms of the ionic liquid products (PDF)

The crystal structure of LIL 4, depicted in Figure 2 (CIF)

■ AUTHOR INFORMATION

Corresponding Authors

Arsalan Mirjafari − *Department of Chemistry and Physics, Florida Gulf Coast University, Fort Myers, Florida 33965, United States;* orcid.org/0000-0002-5502-0602; Email: amirjafari@fgcu.edu

Scott F. Michael − *Department of Biological Sciences, Florida Gulf Coast University, Fort Myers, Florida 33965, United States*; Email: smichael@fgcu.edu

Authors

David J. Siegel − *Department of Chemistry and Physics, Florida Gulf Coast University, Fort Myers, Florida 33965, United States*

Grace I. Anderson − *Department of Chemistry and Physics, Florida Gulf Coast University, Fort Myers, Florida 33965, United States*

Lauren M. Paul − *Department of Biological Sciences, Florida Gulf Coast University, Fort Myers, Florida 33965, United States*

Philipp J. Seibert − *Department of Chemistry and Physics, Florida Gulf Coast University, Fort Myers, Florida 33965, United States*

Patrick C. Hillesheim − *Department of Chemistry and Physics, Ave Maria University, Ave Maria, Florida 34142, United States*

Yinghong Sheng − *Department of Chemistry and Physics, Florida Gulf Coast University, Fort Myers, Florida 33965, United States;* orcid.org/0000-0002-2331-6425

Matthias Zeller − *Department of Chemistry, Purdue University, West Lafayette, Indiana 47907, United States;* orcid.org/0000-0002-3305-852X

Andreas Taubert − *Institute of Chemistry, University of Potsdam, Potsdam D-14476, Germany;* orcid.org/0000-0002-9329-0072

Peter Werner − *Institute of Chemistry, University of Potsdam, Potsdam D-14476, Germany*

Christian Balischewski − *Institute of Chemistry, University of Potsdam, Potsdam D-14476, Germany*

Complete contact information is available at: https://pubs.acs.org/10.1021/acsabm.1c00252

Author Contributions

†D.J.S. and G.I.A. contributed equally. The manuscript was written through contributions of all authors. All authors have given approval to the final version of the manuscript.

Notes

The authors declare no competing financial interest.

■ ACKNOWLEDGMENTS

This material is based upon work supported by the National Science Foundation through the CHE-1952846 (RUI) and CHE-1919785 (MRI) programs. We are grateful for the generous support provided by the Brodie and Blair Foundation Scholarships.

■ REFERENCES

(1) Friedmann, T.; Roblin, R. Gene Therapy for Human Genetic Disease? *Science* **1972**, *175* (4025), 949–955.

(2) Mulligan, R. The basic science of gene therapy. *Science* **1993**, *260* (5110), 926–932.

(3) Francia, V.; Schiffelers, R. M.; Cullis, P. R.; Witzigmann, D. The Biomolecular Corona of Lipid Nanoparticles for Gene Therapy. *Bioconjugate Chem.* **2020**, *31* (9), 2046–2059.

(4) Anguela, X. M.; High, K. A. Entering the Modern Era of Gene Therapy. *Annu. Rev. Med.* **2019**, *70* (1), 273–288.

(5) Zhou, J.; Shao, Z.; Liu, J.; Duan, Q.; Wang, X.; Li, J.; Yang, H. From Endocytosis to Nonendocytosis: The Emerging Era of Gene Delivery. *ACS Applied Bio Materials* **2020**, *3* (5), 2686–2701.

(6) Lynn, D. M.; Anderson, D. G.; Putnam, D.; Langer, R. Accelerated Discovery of Synthetic Transfection Vectors: Parallel Synthesis and Screening of a Degradable Polymer Library. *J. Am. Chem. Soc.* **2001**, *123* (33), 8155–8156.

(7) *Gene Therapy Clinical Trials Worldwide Home Page*. http://www.abedia.com/wiley/phases.php (accessed 2020-08-28).

(8) Buck, J.; Grossen, P.; Cullis, P. R.; Huwyler, J.; Witzigmann, D. Lipid-Based DNA Therapeutics: Hallmarks of Non-Viral Gene Delivery. *ACS Nano* **2019**, *13* (4), 3754–3782.

(9) Kay, M. A. State-of-the-art gene-based therapies: the road ahead. *Nat. Rev. Genet.* **2011**, *12* (5), 316–328.

(10) Zhi, D.; Zhang, S.; Cui, S.; Zhao, Y.; Wang, Y.; Zhao, D. The Headgroup Evolution of Cationic Lipids for Gene Delivery. *Bioconjugate Chem.* **2013**, *24* (4), 487−519.
(11) Wu, Y.; Xiong, Y.; Wang, L.; Zhou, Q.; Li, L.; Levkin, P. A.; Davidson, G.; Gao, L.; Deng, W. Development of new self-assembled cationic amino liposomes for efficient gene delivery. *Biomater. Sci.* **2020**, *8* (11), 3021−3025.
(12) Mohammadinejad, R.; Dehshahri, A.; Sagar Madamsetty, V.; Zahmatkeshan, M.; Tavakol, S.; Makvandi, P.; Khorsandi, D.; Pardakhty, A.; Ashrafizadeh, M.; Ghasemipour Afshar, E.; Zarrabi, A. In vivo gene delivery mediated by non-viral vectors for cancer therapy. *J. Controlled Release* **2020**, *325*, 249−275.
(13) Fink, T. L.; Klepcyk, P. J.; Oette, S. M.; Gedeon, C. R.; Hyatt, S. L.; Kowalczyk, T. H.; Moen, R. C.; Cooper, M. J. Plasmid size up to 20 kbp does not limit effective in vivo lung gene transfer using compacted DNA nanoparticles. *Gene Ther.* **2006**, *13* (13), 1048−1051.
(14) Felgner, P. L.; Gadek, T. R.; Holm, M.; Roman, R.; Chan, H. W.; Wenz, M.; Northrop, J. P.; Ringold, G. M.; Danielsen, M. Lipofection: a highly efficient, lipid-mediated DNA-transfection procedure. *Proc. Natl. Acad. Sci. U. S. A.* **1987**, *84* (21), 7413−7417.
(15) Savarala, S.; Brailoiu, E.; Wunder, S. L.; Ilies, M. A. Tuning the Self-Assembling of Pyridinium Cationic Lipids for Efficient Gene Delivery into Neuronal Cells. *Biomacromolecules* **2013**, *14* (8), 2750−2764.
(16) Draghici, B.; Ilies, M. A. Synthetic Nucleic Acid Delivery Systems: Present and Perspectives. *J. Med. Chem.* **2015**, *58* (10), 4091−4130.
(17) Gaitor, J. C.; Paul, L. M.; Reardon, M. M.; Hmissa, T.; Minkowicz, S.; Regner, M.; Sheng, Y.; Michael, S. F.; Isern, S.; Mirjafari, A. Ionic liquids with thioether motifs as synthetic cationic lipids for gene delivery. *Chem. Commun.* **2017**, *53* (59), 8328−8331.
(18) Laurence, C.; El Ghomari, M. J.; Le Questel, J.-Y.; Berthelot, M.; Mokhlisse, R. Structure and molecular interactions of anti-thyroid drugs. Part 3.1 Methimazole: a diiodine sponge. *J. Chem. Soc., Perkin Trans. 2* **1998**, No. 7, 1545−1552.
(19) O'Brien, R. A.; Zayas, M. S.; Nestor, S. T.; Gaitor, J. C.; Paul, L. M.; Edhegard, F. A.; Minkowicz, S.; Sykora, R. E.; Sheng, Y.; Michael, S. F.; Isern, S.; Mirjafari, A. Biomimetic design of protic lipidic ionic liquids with enhanced fluidity. *New J. Chem.* **2016**, *40* (9), 7795−7803.
(20) Mirjafari, A. Ionic liquid syntheses via click chemistry: expeditious routes toward versatile functional materials. *Chem. Commun.* **2018**, *54* (24), 2944−2961.
(21) Greaves, T. L.; Drummond, C. J. Solvent nanostructure, the solvophobic effect and amphiphile self-assembly in ionic liquids. *Chem. Soc. Rev.* **2013**, *42* (3), 1096−1120.
(22) Canongia Lopes, J. N. A.; Pádua, A. A. H. Nanostructural Organization in Ionic Liquids. *J. Phys. Chem. B* **2006**, *110* (7), 3330−3335.
(23) Burton, R. D.; Siegel, D. J.; Muller, J. E.; Regner, M.; Sheng, Y.; McManus, G. J.; MacDonald, J. H.; Mirjafari, A. From gene delivery agents to ionic liquids: The impacts of cation structure and anion identity on liquefaction. *J. Mol. Liq.* **2019**, *296*, 111758.
(24) McKinnon, J. J.; Mitchell, A. S.; Spackman, M. A. Hirshfeld Surfaces: A New Tool for Visualising and Exploring Molecular Crystals. *Chem. - Eur. J.* **1998**, *4* (11), 2136−2141.
(25) van Bergen, L. A. H.; Alonso, M.; Palló, A.; Nilsson, L.; De Proft, F.; Messens, J. Revisiting sulfur H-bonds in proteins: The example of peroxiredoxin AhpE. *Sci. Rep.* **2016**, *6* (1), 30369.
(26) Lopez-Martin, I.; Burello, E.; Davey, P. N.; Seddon, K. R.; Rothenberg, G. Anion and cation effects on imidazolium salt melting points: a descriptor modelling study. *ChemPhysChem* **2007**, *8* (5), 690−695.
(27) Costa, M. C.; Rolemberg, M. P.; Boros, L. A. D.; Kraehenbuehl, M. A.; de Oliveira, M. G.; Meirelles, A. J. A. Solid-Liquid Equilibrium of Binary Fatty Acid Mixtures. *J. Chem. Eng. Data* **2007**, *52* (1), 30−36.
(28) O'Brien, R. A.; Mirjafari, A.; Mattson, K. M.; Murray, S. M.; Mobarrez, N.; Salter, E. A.; Wierzbicki, A.; Davis, J. H.; West, K. N. The Effect of the Sulfur Position on the Melting Points of Lipidic 1-Methyl-3-Thiaalkylimidazolium Ionic Liquids. *J. Phys. Chem. B* **2014**, *118* (34), 10232−10239.
(29) Rabideau, B. D.; West, K. N.; Davis, J. H. Making good on a promise: ionic liquids with genuinely high degrees of thermal stability. *Chem. Commun.* **2018**, *54* (40), 5019−5031.
(30) Zauner, W.; Ogris, M.; Wagner, E. Polylysine-based transfection systems utilizing receptor-mediated delivery. *Adv. Drug Delivery Rev.* **1998**, *30* (1), 97−113.

https://doi.org/10.1021/acsabm.1c00252
ACS Appl. Bio Mater. 2021, 4, 4737−4743